International Journal of Heat and Mass Transfer 76 (2014) 484–491

Contents lists available at ScienceDirect

International Journal of Heat and Mass Transfer

journal homepage: www.elsevier.com/locate/ijhmt

Mass transfer enhancement during CO_2 absorption process in methanol/Al_2O_3 nanofluids

Jae Hyung Kim [a], Chung Woo Jung [b], Yong Tae Kang [b,*]

[a] Department of Mechanical Engineering, Kyung Hee University, Gyeonggi-do 446-701, Republic of Korea
[b] School of Mechanical Engineering, Korea University, Seoul 136-701, Republic of Korea

ARTICLE INFO

Article history:
Received 2 January 2014
Received in revised form 22 April 2014
Accepted 23 April 2014
Available online 24 May 2014

Keywords:
Al_2O_3 nanoparticles
Bubble motion
CO_2 absorption
Diffusion
Mass transfer

ABSTRACT

The objectives of this paper are to analyze the mass transfer characteristics during CO_2 bubble absorption and diffusion processes in nanofluid with Al_2O_3 nanoparticles. To analyze the effect of the nanoparticles on the mass transfer enhancement, the surface tension and viscosity of the nanofluids are measured. It is found that Al_2O_3 nanoparticles enhance CO_2 absorption rate and increase the viscosity as high as 11% at 0.01 vol% but the surface tension keeps almost constant. The images of bubble absorption and diffusion are captured by a high-speed camera with the shadow-graph method. It is found that the mass transfer coefficient is enhanced up to 26% at 0.01 vol% compared with pure methanol.

1. Introduction

The reduction of greenhouse gases such as CO_2 has become the main issue of global society according to the increasing attention to the environmental issues. For this reason, the integrated gasification combined cycle (IGCC) is getting much attention because of the rich amount of coal around the world and its relative low price. In the IGCC system, it is required to remove the acid gases such as carbon dioxide (CO_2) and hydrogen sulfide (H_2S) for improving the system efficiency [1]. There are several methods to remove CO_2 such as absorption, adsorption, membrane separation, etc. [2]. Among the absorption methods, the Rectisol process, which is a trade name for an acid gas removal process, uses methanol as a solvent to separate the acid gases from the flue gas stream. Methanol can selectively absorb the CO_2 gas [3]. However, the Rectisol process needs very low temperature as low as −40 °C to enhance the CO_2 absorption rate [4]. Therefore, in order to maintain the low temperature, high refrigeration energy consumption is required resulting in high cost.

Most of studies on nanofluids are focused on the thermal conductivity enhancement [5–11]. However, recent studies have shown an enhancement of CO_2 absorption by using nanofluid [12–14]. Therefore, an analysis based on the bubble flow and interaction with the liquid phase is necessary to observe the process of CO_2 absorption. There are many parameters associated with the bubble behavior such as buoyancy, inertial, gravity, viscosity, and drag forces [15], which make it very difficult to investigate the bubble behavior and the nonlinearity accompanied by large deformation of bubbles [16].

In this paper, we visualize the CO_2 bubble absorption process and the diffusion process on the surface in methanol-based nanofluids. Further, we propose a plausible and influential mechanism of mass transfer enhancement through the visualization test and estimate the enhancement of the mass transfer coefficient during the CO_2 bubble absorption process in the methanol-based nanofluids.

2. Experiments

2.1. Experimental setup and preparation of nanofluids

Fig. 1 shows the schematic diagram of the experimental apparatus for the bubble absorption process. The flow rate of CO_2 gas is controlled by a mass flow controller (MFC). A transparent orifice is used to make a single bubble at the bottom of the test section. The temperature of the fluid in the test section is measured by a thermocouple with a measurement error of ±0.4%. The temperature of the nanofluid within the test section is kept 20 °C during the experiment. The solvent is prepared with methanol as a base fluid and Al_2O_3 nanoparticles with different concentrations. The

* Corresponding author. Tel.: +82 2 3290 5952.
E-mail addresses: jaeh@khu.ac.kr (J.H. Kim), funosy97@naver.com (C.W. Jung), ytkang@korea.ac.kr (Y.T. Kang).

http://dx.doi.org/10.1016/j.ijheatmasstransfer.2014.04.057
0017-9310/

Nomenclature

d	diameter, m
E	error, %
Eo	Eotvos number
g	gravity, m/s^2
HSC	high speed camera
k	mass transfer coefficient, m/s
R	radius of CO_2 bubble, m
Re	Reynolds number
r	radius of bubble, m
S	solubility of CO_2 gas
T	temperature, °C
t	time, s
U	uncertainty
V	rising velocity, m/s
X_i	equilibrium concentration at the gas–liquid surface
X	concentration of the bulk liquid
Z	height, m

Greek symbols

ρ	density of CO_2 gas, kg/m^3
μ	viscosity of liquid, mPa s
σ	surface tension of the liquid, N/m

Subscripts

b	bubble
g	gas phase
l	liquid phase
MTC	mass transfer coefficient
ov	overall

nanoparticles are mixed into the methanol with an ultra-sonicator for 60 min. The manufacturing procedure of the methanol-based nanofluids is as follows:

(1) Methanol and nanoparticles are mixed to match the experimental conditions.
(2) Nanoparticles are dispersed in the methanol by an agitator and an ultra-sonicator for 60 min.
(3) Maintain the temperature at 20 °C and is continuously stirred.

The test section is made of hard glass to have a good visualization and to avoid any reaction with the methanol. The concentrations of Al_2O_3 nanoparticles range from 0 to 0.01 vol%. The shadow-graph method is used to visualize the CO_2 bubble behavior. He–Ne laser and Tungsten-Halogen lamp are used as the light source as shown in Fig. 1. The experimental conditions are summarized in Table 1.

2.2. Experimental procedure

The surface tension and viscosity of pure methanol and Al_2O_3 nanofluid are measured by a tensiometer and a viscometer with the experiment errors of 0.001 N/m and 0.006 mPa s, respectively. Two different visualization tests are carried out in this study; CO_2 bubble behavior test and diffusion process test. During the bubble behavior test, a single CO_2 bubble is introduced from the orifice at the bottom of the test section. The mass flow rate of the CO_2 gas is controlled by the MFC. The bubble behavior and shape are captured by a high-speed camera operated at 500 frames/s for 4 s. The pictures of the bubble movement are taken in a shorter time frame due to the fast rising of the bubble. However, the visualization for the surface diffusion process needs more time. The surface absorption and diffusion processes are captured at 60 frames/s for 30 s. Table 2 shows the operating conditions of the high-speed camera. The test section is similar to a Hele–Shaw Cell type. He–Ne laser is spread by a pin-hole and reflected by a mirror. The test section is filled with pure methanol or methanol/Al_2O_3 nanofluid, and the reflected laser passes through the test section. By the difference of scattering degree of the laser in the fluid and gas, the shape of the bubbles can be visualized. During the diffusion test, CO_2 gas is absorbed into the nanofluid surface, and the diffusion process is visualized by the shadow-graph method.

3. Results and discussion

3.1. Surface tension and viscosity measurements

Fig. 2 shows the surface tension and viscosity variations of Al_2O_3 nanofluid at each concentration. The viscosity of the nanofluids is measured by the tuning fork vibration method (Model SV-10), whose rotational speed is 1800 rpm and measurement range is 0.3–10,000 cp(mPa s). The surface tension for pure methanol is estimated as 0.0228 N/m and it decreases down to 0.0226 N/m in nanofluid, only by decrease of 0.8%. Therefore, it is concluded that the surface tension force gives a very small or no

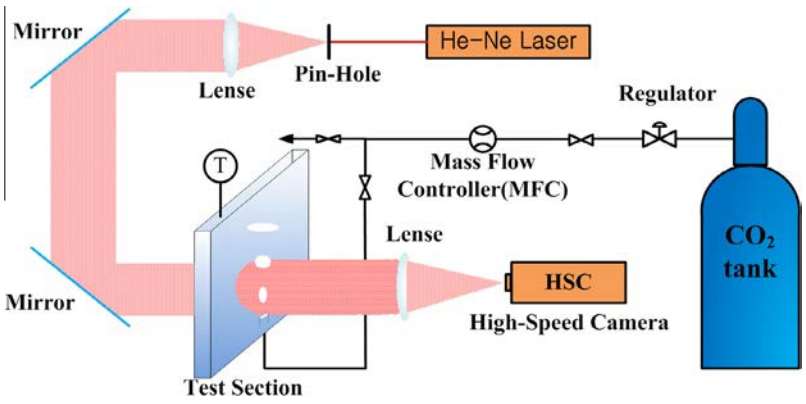

Fig. 1. Schematic diagram of the experimental apparatus for the CO_2 bubble absorption process.

Table 1
Experiment conditions.

Base fluid	Methanol	
Nanoparticle	Al_2O_3	
Size of nanoparticle [nm]	40–50	
Vapor	CO_2	
Volume fraction of Al_2O_3 [vol%]	0, 0.001, 0.005, 0.01	
Test section [mm]	200 × 200 × 5	
	200 × 200 × 1	
Fluid temp [°C]	20	
Ultra-sonicator	Time [min]	60
	Frequency [kHz]	20
	Power [W]	350
	Pulse [s]	2
	Term [s]	1

Table 2
Experiments.

	Bubble behavior test	Diffusion test
Recording time [s]	4	30
Recording speed [frames/s]	500	60
Exposure [EV]	60–150	

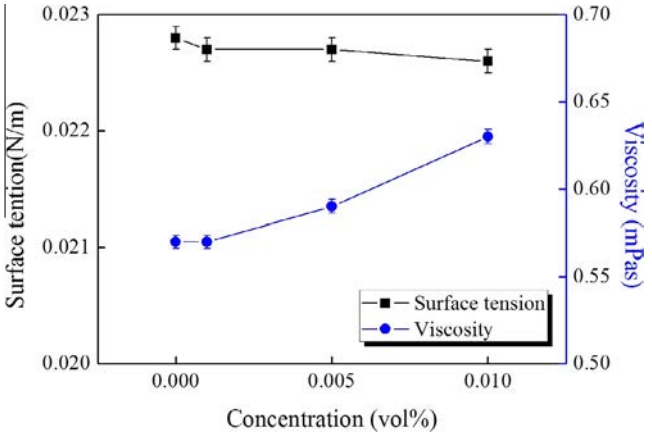

Fig. 2. Surface tension and viscosity at each concentration.

effect on the bubble behavior. On the other hand, the viscosity of pure methanol is estimated as 0.57 mPa s and the viscosity of the nanofluid increases up to 0.63 mPa s for the highest concentration, which is 11% higher than that of the pure methanol. These results are similar to the other research of nanofluid [17–20].

3.2. Bubble shape and behavior

Fig. 3 shows the single bubble behavior in pure methanol and methanol-based nanofluids with Al_2O_3 nanoparticles, taken by the shadow graph method. The bubble size becomes smaller as the concentration of Al_2O_3 increases from the point where the bubble detaches. By comparing the location of the bubbles and the number of frames, it is possible to calculate the bubble rising velocity. Fig. 4 shows the bubble rising velocity at each concentration. It is found that the bubble is not broken out, but absorbed from the orifice, so the initial bubble size becomes smaller with increasing the concentration of nanoparticles, which means the enhancement of absorption performance in nanofluids.

Figs. 5 and 6 show the bubble rising and absorption processes in pure methanol and methanol-based nanofluids with Al_2O_3 nanoparticles, respectively. In Fig. 3, the CO_2 absorption starts to occur within the orifice so that the absorption enhancement by

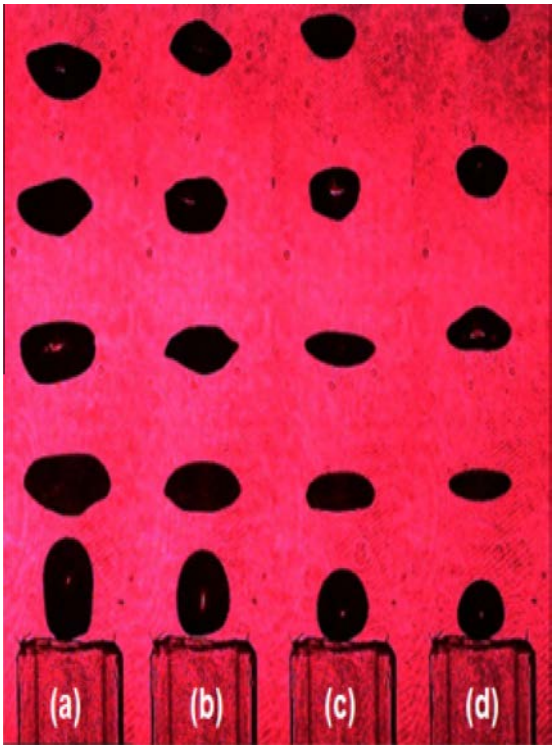

Fig. 3. High-speed camera pictures of CO_2 bubbles in (a) pure methanol, and methanol/Al_2O_3 mixture at (b) 0.001 vol%, (c) 0.005 vol%, (d) 0.01 vol%.

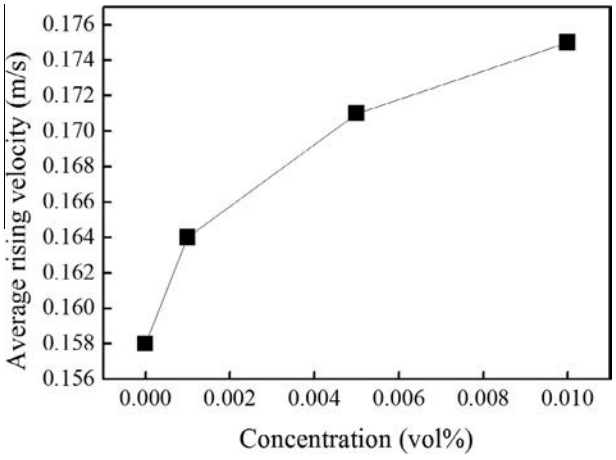

Fig. 4. Bubble rising velocity at each concentration.

nanoparticles can be visualized by comparing the initial bubble diameter and the bubble rising velocity. In Figs. 5 and 6, the test section is designed as the Hele–Show type flow to have similar initial bubble diameters for each case, and then the bubble sizes are compared during the absorption process after the initial bubble diameter. To analyze the effect of nanoparticles on the bubble shape and the rising velocity, pure methanol and the highest concentration of methanol + Al_2O_3(0.01 vol%) mixture are compared. The interval of each picture is 0.104 s and they are put together in one picture. The thickness of the bubble shadow line is considered as the allowable error in the calculation of the size. The rising velocity of the bubble is calculated by the number of frames of the high speed camera.

Fig. 7 shows the results of the CO_2 bubble size variation for both cases. It is found that the bubble size in methanol decreases about 43% compared with the initial bubble, while the bubble size in

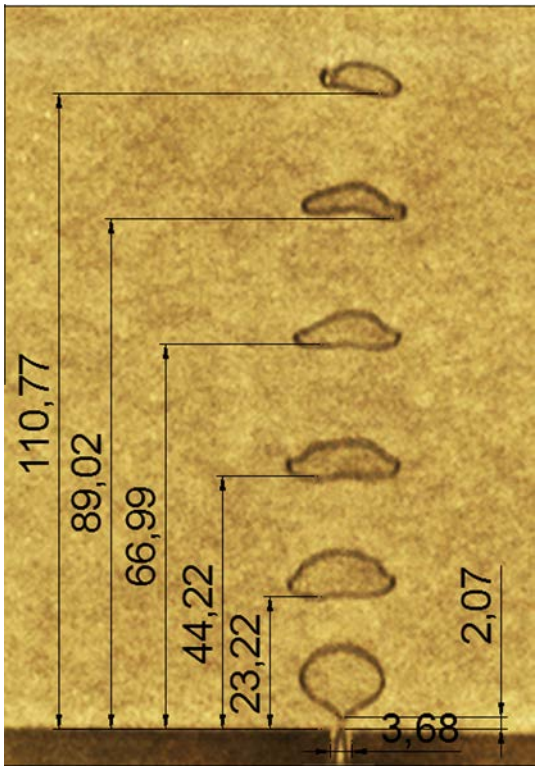

Fig. 5. The variation of CO_2 bubble behavior in methanol.

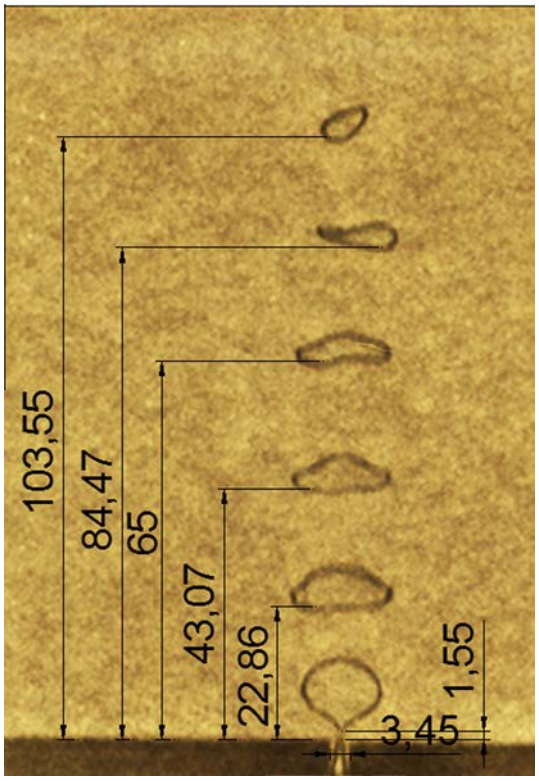

Fig. 6. The variation of CO_2 bubble behavior in methanol + Al_2O_3(0.01 vol%).

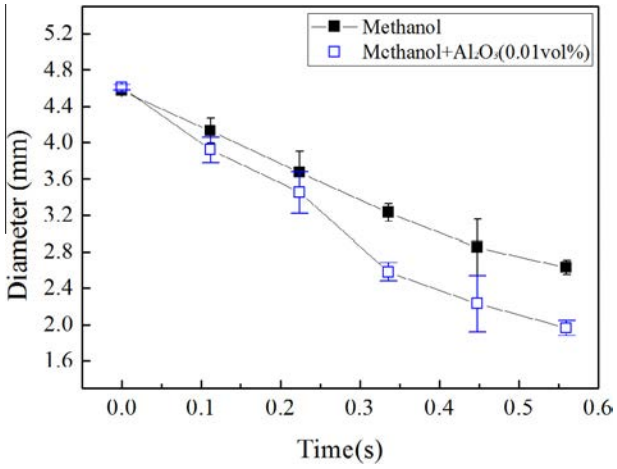

Fig. 7. The variation of CO_2 bubble diameter.

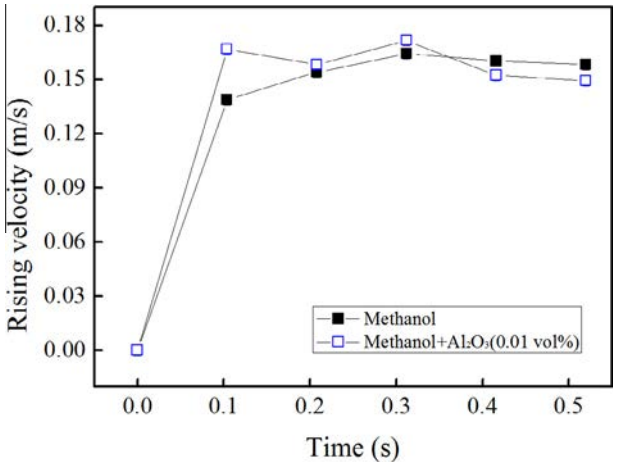

Fig. 8. The variation of CO_2 bubble rising velocity at each step.

Table 3
Bubble state in methanol.

Methanol & CO2						
T (s)	d (mm)	Δd (mm)	Z (mm)	ΔZ (mm)	V_b (m/s)	$K_l \times 10^4$
0	4.57	–	1.68	–	–	–
0.112	4.07	0.50	17.24	15.55	0.13	8.17
0.224	3.56	0.51	34.51	17.27	0.15	8.36
0.336	3.19	0.37	52.92	18.40	0.16	6.05
0.448	2.88	0.30	70.88	17.95	0.16	4.94
0.560	2.59	0.29	88.61	17.73	0.15	4.84

Table 4
Bubble state in methanol + Al_2O_3(0.01 vol%).

Methanol + Al_2O_3(0.01 vol%) & CO_2						
T (s)	d (mm)	Δd (mm)	Z (mm)	ΔZ (mm)	V_b (m/s)	$K_l \times 10^4$
0	4.65	–	1.35	–	–	–
0.112	3.92	0.73	20.05	18.69	0.16	11.97
0.224	3.30	0.62	37.78	17.72	0.15	10.25
0.336	2.73	0.56	57.01	19.23	0.17	9.27
0.448	2.23	0.50	74.09	17.07	0.15	8.18
0.560	1.88	0.34	90.83	16.73	0.14	5.67

methanol + Al_2O_3(0.01 vol%) mixture decreases about 60% compared with the initial bubble. Fig. 8 shows the variation of CO_2 bubble rising velocity at each step. When the bubble is detached, the bubble velocity changes at each section and it gradually converges to the terminal velocity. Tables 3 and 4 show

the results of the bubble size and rising velocity measurement during the absorption process in methanol and methanol + Al_2O_3(0.01 vol%) mixture based on Figs. 7 and 8. The bubble diameters for pure methanol and nanofluid range 4.57–2.63 and 4.61–1.96 mm for given time period, respectively.

3.3. Mass transfer coefficient

Mass transfer coefficient during the CO_2 bubble absorption process is calculated by an empirical formula for mass transfer between bubble and liquid [21].

$$\frac{dZ}{dR} = \frac{\rho_g V_b}{\rho_l k_l (X_i - X)} \tag{1}$$

where, k_l is the mass transfer coefficient, Z and R are the rising height and the CO_2 bubble radius. X_i and X are the equilibrium concentration of the CO_2 at the gas–liquid surface and concentration of the bulk liquid. Also, the bubble absorption process could be expressed by following mass balance equation [22].

$$\left| \frac{d}{dt}\left(\frac{4}{3}\pi r^3 X\right) \right| = 4\pi r^2 k_{ov}(X_i - X) \tag{2}$$

where, k_{ov} is the overall mass transfer coefficient, r is the radius of the bubble. It is assumed that the concentration of CO_2 at the bulk liquid (X) is zero, because initially there is no CO_2 in the liquid. The concentration of CO_2 at the vapor–liquid surface is estimated by the previous research [13]. The following equation is obtained by rearranging equation (1) to calculate the mass transfer coefficient.

$$k_l = \left(\frac{dR}{dZ}\right)\left(\frac{\rho_g}{\rho_l}\right)\left(\frac{V_b}{X_i - X}\right) \tag{3}$$

The mass transfer coefficient at each step can be calculated based on the results of Tables 3 and 4. Fig. 9 shows the variation of the corresponding mass transfer coefficient. There is a reversal point at 0.2 s that could be caused by the bubble vibration and the wall effect by the relatively low viscosity of the pure methanol. The mass transfer coefficients for pure methanol and nanofluid range 8.17–4.84 and 11.97–5.67 for given time period, respectively. It is found that the mass transfer coefficient enhances up to 26% in average in the nanofluids.

3.4. Uncertainty analysis

The experimental uncertainty in the measurement of the mass transfer coefficient could be estimated by the following Eq. (4).

$$U = \sqrt{\left(\frac{E_{R_{max}}}{R_{max}}\right)^2 + \left(\frac{E_{S_{max}}}{S_{max}}\right)^2 + \left(\frac{E_{T_{max}}}{T_{max}}\right)^2} \tag{4}$$

where U and E are experimental uncertainty and experimental errors for each parameter; bubble diameter, solubility and temperature. The experimental uncertainties for bubble diameter, solubility and temperature are estimated as 8.1%, 2.2% and 0.04%, respectively. The total experimental uncertainty in the measurement of the mass transfer coefficient is estimated as 8.4%.

3.5. Dimensionless numbers

Considering the CO_2 gas bubble rising process in liquid, its behavior will depend on the physical properties of the liquid and vapor such as density, viscosity, surface tension and so on. In this paper, the Reynolds number, Re and the Eotvos number, Eo are considered as the important parameters which are defined as follows;

$$\mathrm{Re} = \frac{\rho V_b d_b}{\mu} \tag{5}$$

$$\mathrm{Eo} = \frac{\rho d_b^2 g}{\sigma} \tag{6}$$

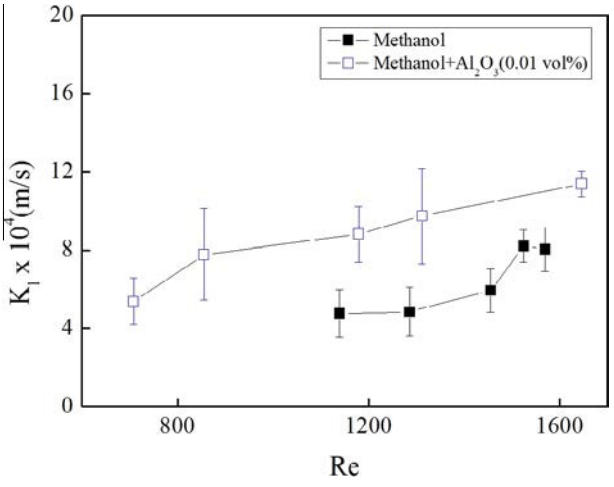

Fig. 10. The variation of the mass transfer coefficient and Reynolds number.

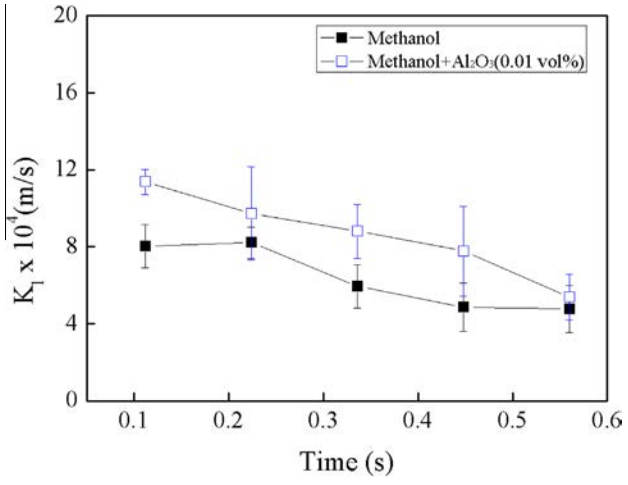

Fig. 9. The variation of the mass transfer coefficient.

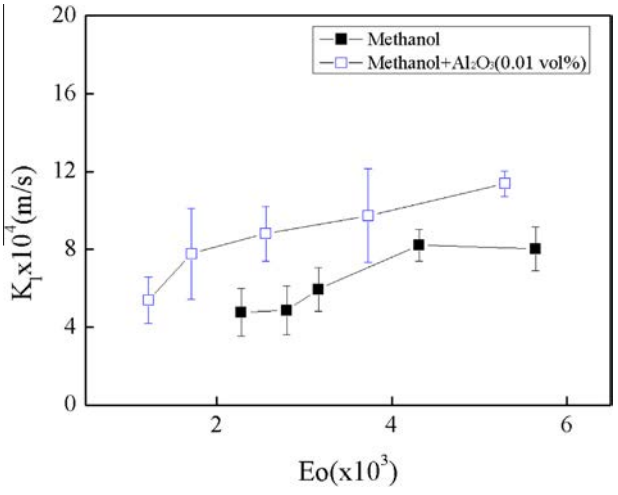

Fig. 11. The variation of the mass transfer coefficient and Eotvos number.

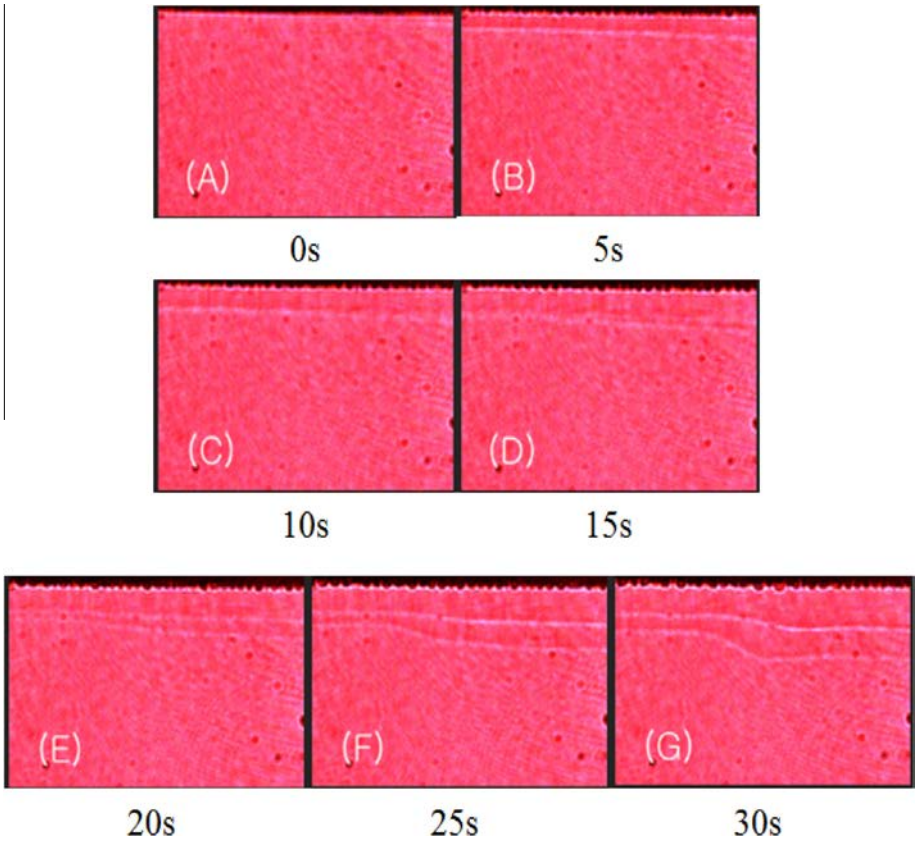

Fig. 12. Diffusion process in pure methanol, A: 0 s, B: 5 s, C: 10 s, D: 15 s, E: 20 s, F: 25 s, G: 30 s.

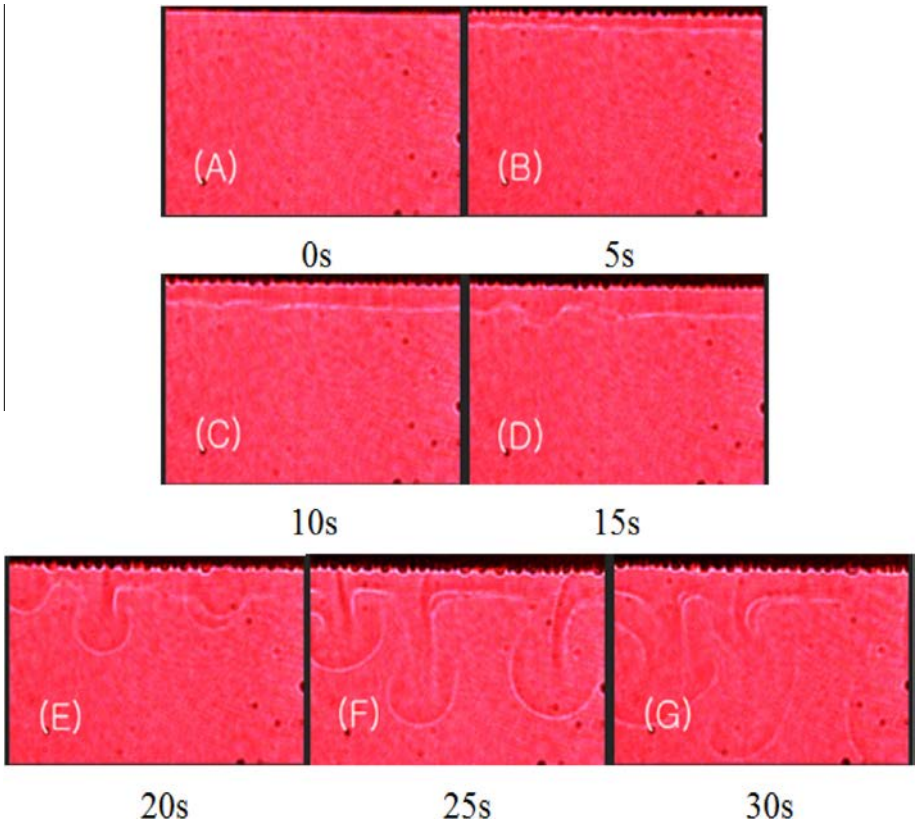

Fig. 13. Diffusion process in methanol + Al_2O_3(0.01 vol%), A: 0 s, B: 5 s, C: 10 s, D: 15 s, E: 20 s, F: 25 s, G: 30 s.

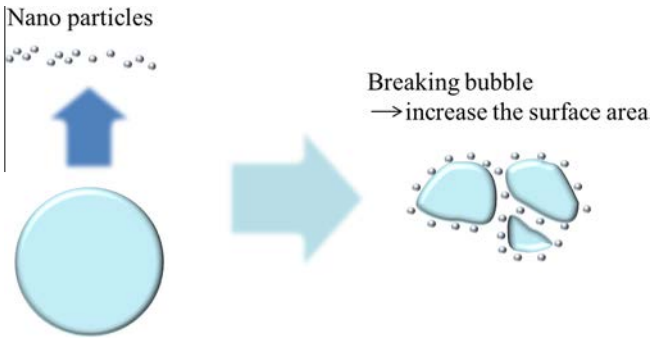

Fig. 14. The schematic diagram of the bubble breaking effect.

Fig. 10 shows the variation of mass transfer coefficient as a function of Re. It is found that the mass transfer coefficient increases with increasing Re. In the present study, Re mainly depends on the variation of bubble diameter. We could expect that the nanoparticles surrounding the bubble enhance the surface roughness due to the hydrodynamic effect. The increment of the surface roughness reduces the drag force by pushing it back to the flow separation point and thus increases the contact area. It means that the absorption rate increases by adding the nanoparticles in the liquid. Fig. 11 shows the variation of mass transfer coefficient as a function of Eo. It is found that the mass transfer coefficient increases with increasing Eo. The Eotvos number is basically related with the volume of the bubble. It means that the Eotvos number represents how the mass transfer changes with the volume variation of the bubble. It is found that the mass transfer coefficient increases with increasing the bubble diameter as shown in Tables 3 and 4.

3.6. Diffusion boundary layer

Fig. 12 shows the visualization results for the diffusion process in pure methanol. The CO_2 gas is absorbed at the liquid surface. As can be seen in Fig. 12, CO_2 gas is absorbed and diffused like a

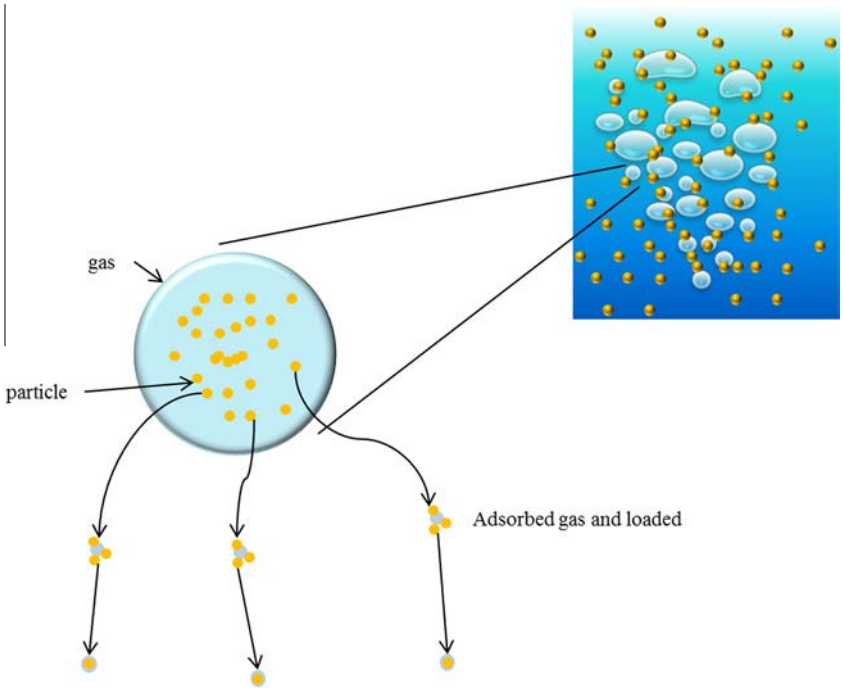

Fig. 15. The schematic diagram of the shuttle effect.

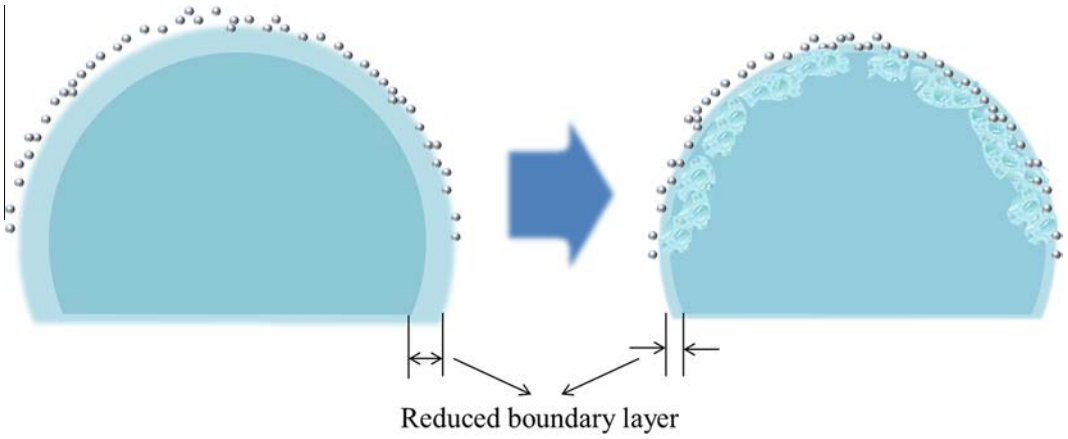

Fig. 16. The schematic diagram of the hydrodynamic effect.

laminar flow motion. On the other hand, we can see the turbulent flow motion like a mushroom in methanol + Al_2O_3(0.01 vol%) as shown in Fig. 13. The time interval is set to be 5 s. It could be considered that the diffusion boundary layer is broken and decreased by the nano particles within the liquid. It could be explained by the hydrodynamic effect mechanism, which is explained in more detail in the next section. When the CO_2 gas is absorbed into the solution, the nanoparticles are concentrated around the surface, and the CO_2 molecules diffuse faster by the nanoparticles. The diffusion boundary layer becomes thinner by the nanoparticles motion and then CO_2 is diffused faster than that in pure methanol, resulting in the enhancement of CO_2 absorption rate.

3.7. Mass transfer enhancement mechanisms

Fig. 14 shows the bubble breaking effect mechanism. During the bubble absorption process, the nanoparticles collide against each other and against the bubble. As the bubble rises up and the motion become more dynamic, the nanoparticles collide at the gas–liquid interface, and finally break the bubbles. The bubbles become smaller and the interfacial area becomes larger, resulting in the enhancement of mass transfer. We call this the "bubble breaking effect". However, it is found that the bubbles are not broken as shown in Fig. 3. Therefore, the bubble breaking mechanism does not seem to be plausible.

Fig. 15 shows the shuttle effect mechanism. The shuttle effect occurs during the transport process of gas by nanoparticles in the liquid. Nanoparticles are cycling in the liquid and the CO_2 gas is adsorbed by the particles at the gas–liquid surface. The adsorbed gas by the nanofluid is moved from a high concentration region to a low concentration region. The nanoparticles move back to the original place to adsorb the CO_2 gas again. The surface and internal flow becomes more dynamic leading to the enhancement of mass transfer. We call this phenomenon the "shuttle effect mechanism" [23]. However, it is very difficult to estimate quantitatively the effect of the shuttle effect mechanism on the CO_2 absorption performance in the present study because the concentration of nanoparticles is very low.

Fig. 16 shows the hydrodynamic effect mechanism. In the hydrodynamic effect, the nanoparticles surrounding the bubbles break the diffusion boundary layer and make it thinner. Diffusion into the liquid film increases by the presence of the particles near the interface between the bubble and the liquid. We call this the "hydrodynamic effect mechanism".

4. Conclusions

In this study, we visualized the CO_2 bubble behavior in absorption and diffusion processes with methanol based Al_2O_3 nanofluid, and measured the mass transfer coefficient during the CO_2 absorption process. The following conclusions are drawn from the present study.

(1) The surface tension of methanol + Al_2O_3 nanofluid at 0.01 vol% decreases but only by 0.8%. On the other hand, the viscosity of the nanofluid increases up to 11% compared with the pure methanol.
(2) It is found that the mass transfer coefficient increases about 26% at 0.01 vol% in nanofluid compared with the base fluid.
(3) During the mass diffusion process in the nanofluid, turbulent motion like mushroom shape is found, which is a strong evidence to propose the hydrodynamic effect mechanism in the mass transfer enhancement.
(4) It is concluded that the nanoparticles enhance the mass transfer and that the hydrodynamic effect is a more plausible mechanism than other effects to explain the mass transfer enhancement in nanofluid.

Conflict of interest

None declared.

Acknowledgment

This work was supported by the National Research Foundation (NRF) South Korea Grant (No. 2010-0029120) funded by Korean Government (MEST).

References

[1] K. Christian, R. Karsten, S. Hartmut, Structured exergy analysis of an integrated gasification combined cycle (IGCC) plant with carbon capture, Int. J. Energy Res. 36 (2011) 1480–1487.
[2] J.D. Figueroa, T. Fout, S. Plasynsky, H. McIlvried, R.D. Srivastava, Advances in CO_2 capture technology – the U.S department of energy's carbon sequestration program, Int. J. Greenhouse Gas Control 2 (2008) 9–20.
[3] N. Korens, D.R. Simbeck, D.J. Wilgelm, Process screening analysis of alternative gas treating and sulfur removal for gasification, Prepared for U.S. Department of Energy by SFA Pacific, Inc., Revised Final Report, 2002.
[4] G. Ranke, V.H. Mogr, The rectisol wash: new developments in acid gas removal from synthesis gas, from acid and sour gas treating processes, in: Stephen A. Newman, (Ed.), Gulf Publishing Company, Houston, 1985, pp. 80–111.
[5] S. Lee, S.U. Choi, S. Li, JA. Eastman, Measuring thermal conductivity of fluids containing oxide nanoparticles, ASME J. Heat Transfer 121 (1999) 280–289.
[6] J.A. Eastman, S.U. Choi, W. Yu, I.J. Thompson, Anomalously increased effective thermal conductivity of ethylene glycol-based nanofluids containing copper nanoparticles, Appl. Phys. Lett. 78 (2001) 718–720.
[7] S.U.S. Choi, Z.G. Zhang, W. Yu, F.E. Lockwood, E.A. Grulke, Anomalous thermal conductivity enhancement in nanotube suspensions, Appl. Phys. Lett. 79 (2001) 2252–2254.
[8] S.K. Das, N. Putra, P. Thuesem, W. Roetzel, Temperature dependence of thermal conductivity enhancement for nanofluids, ASME J. Heat Transfer 125 (2003) 567–574.
[9] H.E. Patel, S.K. Das, T. Sundararajan, A.S. Narr, B. George, T. Pradeep, Thermal conductivities of naked and monolayer protected metal nanoparticle base nanofluids: manifestation of anomalous enhancement and chemical effects, Appl. Phys. Lett. 83 (2004) 2931–2933.
[10] S.P. Jang, S.U.S. Choi, The role of Brownian motion in the enhanced thermal conductivity of nanofluids, Appl. Phys. Lett. 84 (21) (2004) 4316–4318.
[11] S.M. Kwark, M. Amaya, S.M. You, Experimental pool boiling heat transfer study of the nanoporous coating in various fluids, Int. J. Air-Conditioning Refrig. 20 (2012) 1150001.
[12] W.G. Kim, H.U. Kang, K.M. Jung, S.H. Kim, Synthesis of silica nanofluid and application to CO_2 absorption, Sep. Sci. Technol. 43 (2008) 3036–3055.
[13] J.W. Lee, J.Y. Jung, S.G. Lee, Y.T. Kang, CO_2 bubble absorption enhancement in methanol-based nanofluids, Int. J. Refrig. 34 (2011) 1727–1733.
[14] I. Torres Pineda, J.W. Lee, I.H. Jung, Y.T. Kang, CO_2 absorption enhancement by methanol-based Al_2O_3 and SiO_2 nanofluids in a tray column absorber, Int. J. Refrig. 35 (2012) 1402–1409.
[15] Z. Cai, Y. Bao, Z. Gao, Hydrodynamic behavior of a single bubble rising in viscous liquids. Fluid flow and transport phenomena, J. Chem. Eng. 18 (6) (2010) 923–930. Chinese.
[16] H. Wang, Z. Zhang, Y. Yang, H. Zhang, Viscosity effects on the behavior of a rising bubble, J. Hydrodyn. 22 (1) (2010) 81–89.
[17] M. Chandrasekar, S. Suresh, A. Chandra Bose, Experimental investigations and theoretical determination of thermal conductivity and viscosity of Al_2O_3/water nanofluid, Exp. Therm. Fluid Sci. 34 (2010) 210–216.
[18] S.M.S. Murshed, K.C. Leong, C. Yang, Investigations of thermal conductivity and viscosity of nanofluids, Int. J. Therm. Sci. 47 (2008) 560–568.
[19] S.K. Das, N. Putra, W. Roetzel, Pool boiling characteristics of nanofluids, Int. J. Heat Mass Transfer 46 (2003) 851–862.
[20] A. Kaya, A. Schumpe, Surfactant adsorption rather than "shuttle effect"?, Chem Eng. Sci. 60 (2005) 6504–6510.
[21] R.E. Treybal, Mass-transfer Operations, McGraw-Hill, New York, 1980. p. 139.
[22] A. Yanasaki, K. Ogasawara, H. Teng, Mass transfer from CO_2 drops traveling in high-pressure and low-temperature water, Energy Fuel 15 (2001) 147–150.
[23] J.H.J. Kluyrmans, B.G.M. Van Wachem, B.F.M. Kuster, J.C. Schouten, Mass transfer in sparged and stirred reactors: influence of carbon particles and electrolyte, Chem. Eng. Sci. 58 (2002) 4719–4728.